

Optimal unidirectional amplification induced by optical gain in optomechanical systems

L. N. Song¹, Qiang Zheng^{2,1,*}, Xun-Wei Xu³, Cheng Jiang^{1,4}, and Yong Li^{1,5†}

¹ *Beijing Computational Science Research Center, Beijing 100193, China*

² *School of Mathematics, Guizhou Normal University, Guiyang 550001, China*

³ *Department of Applied Physics, East China Jiaotong University, Nanchang 330013, China*

⁴ *School of Physics and Electronic Electrical Engineering, Huaiyin Normal University, Huai'an 223300, China and*

⁵ *Synergetic Innovation Center for Quantum Effects and Applications, Hunan Normal University, Changsha 410081, China*

(Dated: January 6, 2022)

We propose a three-mode optomechanical system to realize optical nonreciprocal transmission with unidirectional amplification, where the system consists of two coupled cavities and one mechanical resonator which interacts with only one of the cavities. Additionally, the optical gain is introduced into the optomechanical cavity. It is found that for a strong optical input, the optical transmission coefficient can be greatly amplified in a particular direction and suppressed in the opposite direction. The expressions of the optimal transmission coefficient and the corresponding isolation ratio are given analytically. Our results pave a way to design high-quality nonreciprocal devices based on optomechanical systems.

PACS numbers: 42.60.Lh, 42.65.Yj, 42.50.Vk

I. INTRODUCTION

The study of optomechanical systems [1] based on the parametric coupling between the photonic and phononic fields, excites a wide range of interests. Many interesting properties of the optomechanical systems, such as optomechanically induced transparency (OMIT) [2–4], quantum entanglement [5, 6], Bell-nonlocality [7], and imaging structure of tumors [8], have been reported. These properties indicate that the optomechanical system is a key quantum coherent device for precise measurement and quantum information processing.

In a network based on electrical or optical elements, one of the key coherent devices is the nonreciprocal one, such as isolator or circulator, where the signals have significantly different transmission behaviors in two opposite directions due to the breaking of time-reversal symmetry. Traditionally, the approach to break the time-reversal symmetry is utilizing the magneto-optical effect [9, 10], which usually makes the system bulky and unrobust to the external magnetic field. Recently, several magnetic-free mechanisms have been proposed to implement nonreciprocal devices, such as spatio-temporal asymmetry of refractive-index [11, 12], angular momentum biasing in photonic or acoustic systems [13–16].

As an all-optical and magnetic-free platform, the optomechanical system has also been suggested to implement the optical nonreciprocal devices. Up to now, there exist at least two kinds of optical nonreciprocity based on optomechanical systems. For the first kind, the transmitted signal is the weak light field, and its transmis-

sion behavior is assisted by another strong control field which enhances significantly the effective optomechanical coupling. This kind of nonreciprocity has been achieved in physical systems displayed OMIT [17–19], frequency conversion between optical and microwave fields [20, 21], and quantum-limited amplification [22–31]. And the second kind of optical nonreciprocity is based on the nonlinear interaction in the system, suggested in Ref. [32]. Here the input field (that is, the transmitted signal) is usually very strong, and it is not necessary to introduce the additional strong control field. A variety of nonlinear interactions, induced by coupling the cavity fields to a qubit [33], atomic ensemble [34, 35], mechanical resonators [36–38], Brillouin scattering [39–41], or nonlinear optical medium [42], have been used to investigate this kind of optical nonreciprocity.

We would like to note that a nonreciprocal device of optical diode based on the nonlinear interaction has recently been proposed [38] in a three-mode system, which is composed by a standard optomechanical system plus another cavity coupled with the optomechanical cavity (shown in Fig. 1). In this work, we will further investigate the optical nonreciprocal phenomenon in the similar three-mode optomechanical system with introducing an additional optical gain for the optomechanical cavity.

For the case without optical gain [38], the value of the transmission coefficient is usually smaller than 1 and the optical diode was achieved. With the aid of the optical gain in the three-mode optomechanical system, we find in this work that the value of the transmission coefficient in one direction can be much larger than 1, while in the opposite direction it can be much smaller than 1. Thus, the optical unidirectional amplification can be achieved with good isolation rate due to the presence of the additional optical gain. And the analytical expression of the opti-

* qz@gznu.edu.cn

† liyong@csrc.ac.cn

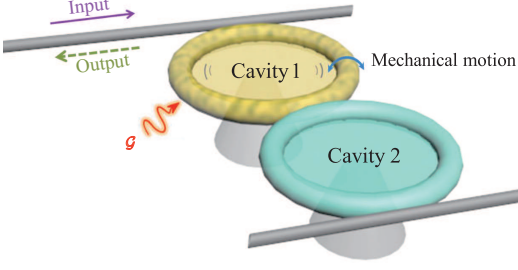


FIG. 1. (Color online) Schematic diagram of the three-mode optomechanical system with optical gain. The whispering-gallery cavity 1 is coupled to the mechanical mode induced by radial radiation-pressure onto the cavity boundary [43], and the additional optical gain \mathcal{G} is introduced for cavity 1 [42, 44]. The second whispering-gallery cavity 2 is coupled to the cavity 1 via optical hopping interaction. The input field is injected either from the cavity 1 or the cavity 2.

mal transmission coefficient in the amplifying direction is obtained, which is only determined by the product of two factors, with the first (second) term representing the proportion of the external decay rate into the effective (total) decay of the cavity.

II. MODEL AND STEADY-STATE SOLUTION

For concreteness, the optomechanical system under consideration is schematically shown in Fig. 1, which consists of two coupled whispering-gallery cavities and one mechanical resonator induced by radial radiation-pressure onto the cavity boundary [43] of one of the cavities (cavity 1). In addition, the optical gain is introduced for cavity 1, which can be achieved by doped Er^{3+} ions in silica with pumping the Er^{3+} ions by a laser [42, 44]. The Hamiltonian of such an optomechanical system can be written as ($\hbar = 1$)

$$H = \omega_1 a_1^\dagger a_1 + \omega_2 a_2^\dagger a_2 + \frac{1}{2} \omega_m (q^2 + p^2) + J(a_1^\dagger a_2 + a_2^\dagger a_1) + g a_1^\dagger a_1 q + i \sqrt{\kappa_{1,e}} \left(\alpha_{1,\text{in}} a_1^\dagger e^{-i\omega_d t} - \alpha_{1,\text{in}}^* a_1 e^{i\omega_d t} \right) + i \sqrt{\kappa_{2,e}} \left(\alpha_{2,\text{in}} a_2^\dagger e^{-i\omega_d t} - \alpha_{2,\text{in}}^* a_2 e^{i\omega_d t} \right), \quad (1)$$

where a_1 and a_2 are the annihilation operators of the optical fields in two cavities (with the frequencies of ω_1 and ω_2); p and q are the momentum and displacement operators of the mechanical resonator (with the resonance frequency of ω_m), respectively. $\kappa_{j,e}$ ($j = 1, 2$) is the external decay rate of cavity j . In Eq. (1), the fourth term denotes the coupling between two cavities with strength J , and the fifth term represents the radiation-pressure optomechanical coupling with the single-photon optomechanical coupling g . The last two terms stand for the coupling between the classical input fields (with the amplitude $\alpha_{j,\text{in}}$ and the frequency of ω_d) and the cavity fields.

According to Hamiltonian (1), the quantum Langevin equations (QLEs) are obtained in the rotating frame of the driving frequency ω_d as

$$\dot{a}_1 = - \left(i\Delta_1 + \frac{\kappa_{\text{eff}}}{2} \right) a_1 - igqa_1 - iJa_2 + \sqrt{\kappa_{1,e}}\alpha_{1,\text{in}} + \sqrt{\kappa_{1,e}}a_{1,\text{in}}^{(e)} + \sqrt{\kappa_{1,o}}a_{1,\text{in}}^{(o)} + \sqrt{\mathcal{G}}a_{1,\text{in}}^{(g)}, \quad (2a)$$

$$\dot{a}_2 = - \left(i\Delta_2 + \frac{\kappa_2}{2} \right) a_2 - iJa_1 + \sqrt{\kappa_{2,e}}\alpha_{2,\text{in}} + \sqrt{\kappa_{2,e}}a_{2,\text{in}}^{(e)} + \sqrt{\kappa_{2,o}}a_{2,\text{in}}^{(o)}, \quad (2b)$$

$$\dot{q} = \omega_m p, \quad (2c)$$

$$\dot{p} = -\omega_m q - ga_1^\dagger a_1 - \gamma_m p + \sqrt{2\gamma_m}\zeta, \quad (2d)$$

where $\Delta_j = \omega_j - \omega_d$ ($j = 1, 2$) is the detuning of cavity j from the input field, respectively. $\kappa_j = \kappa_{j,o} + \kappa_{j,e}$ is the total decay rate of cavity j , where $\kappa_{j,o}$ is the intrinsic decay rate. $\kappa_{\text{eff}} = \kappa_1 - \mathcal{G}$ is the effective decay rate of cavity 1, where \mathcal{G} is the gain rate induced by the doped Er^{3+} ions with optical pumping. γ_m is the decay rate of the mechanical resonator, $a_{j,\text{in}}^{(e)}$, $a_{j,\text{in}}^{(o)}$, $a_{1,\text{in}}^{(g)}$, and ζ are the noise operators with zero mean values.

Assuming the input signal field(s) to be strong enough, the operators can be replaced by their average values with the mean-field approximation $\alpha_j = \langle a_j \rangle$, $\alpha_{j,\text{in}} = \langle a_{j,\text{in}} \rangle$, $\bar{p} = \langle p \rangle$, and $\bar{q} = \langle q \rangle$. From Eqs. (2a-2d), one can obtain the following steady-state equations

$$0 = - \left(i\Delta_1 + \frac{\kappa_{\text{eff}}}{2} \right) \alpha_1 - ig\bar{q}\alpha_1 - iJ\alpha_2 + \sqrt{\kappa_{1,e}}\alpha_{1,\text{in}}, \quad (3a)$$

$$0 = - \left(i\Delta_2 + \frac{\kappa_2}{2} \right) \alpha_2 - iJ\alpha_1 + \sqrt{\kappa_{2,e}}\alpha_{2,\text{in}}, \quad (3b)$$

$$\bar{p} = 0, \quad (3c)$$

$$\bar{q} = - \frac{g|\alpha_1|^2}{\omega_m}. \quad (3d)$$

To study the optical nonreciprocal transmission, we will focus on two cases. In the first case, the input field is only injected into cavity 1 with amplitudes $|\alpha_{1,\text{in}}| = \sqrt{p_{\text{in}}/(\hbar\omega_d)}$ and $\alpha_{2,\text{in}} = 0$, where p_{in} is the power of the input field. With the input-output relation [45]

$$\alpha_{j,\text{out}} + \alpha_{j,\text{in}} = \sqrt{\kappa_{j,e}}\alpha_j, \quad (4)$$

the equation of the output field $\alpha_{2,\text{out}}$ can be given as

$$0 = - \left(\frac{\kappa}{2} + i\Delta \right) \alpha_{2,\text{out}} + iU|\alpha_{2,\text{out}}|^2 \alpha_{2,\text{out}} + \varepsilon\alpha_{1,\text{in}}, \quad (5)$$

where

$$\kappa \equiv \kappa_{\text{eff}} + \frac{4J^2\kappa_2}{\kappa_2^2 + 4\Delta_2^2}, \quad (6a)$$

$$\Delta \equiv \Delta_1 - \frac{4J^2\Delta_2}{\kappa_2^2 + 4\Delta_2^2}, \quad (6b)$$

$$U \equiv \frac{g^2(\kappa_2^2 + 4\Delta_2^2)}{4\omega_m J^2 \kappa_{2,e}}, \quad (6c)$$

$$\varepsilon \equiv -\frac{2iJ\sqrt{\kappa_{1,e}\kappa_{2,e}}}{\kappa_2 + 2i\Delta_2}. \quad (6d)$$

In the second case, the input field is only injected into cavity 2 with the amplitude $|\tilde{\alpha}_{2,\text{in}}| = \sqrt{\tilde{p}_{\text{in}}/(\hbar\omega_d)}$ and $\tilde{\alpha}_{1,\text{in}} = 0$, where \tilde{p}_{in} is the power of input field. Here we have added tildes “ \sim ” for $\alpha_{j,\text{in}}$, $\alpha_{j,\text{out}}$, and p_{in} in order to distinguish them from that in the first case.

Similarly, the equation of the output field $\tilde{\alpha}_{1,\text{out}}$ is obtained as

$$0 = -\left(\frac{\kappa}{2} + i\Delta\right)\tilde{\alpha}_{1,\text{out}} + i\tilde{U}|\tilde{\alpha}_{1,\text{out}}|^2\tilde{\alpha}_{1,\text{out}} + \varepsilon\tilde{\alpha}_{2,\text{in}}, \quad (7)$$

where

$$\tilde{U} \equiv \frac{g^2}{\omega_m \kappa_{1,e}}. \quad (8)$$

To describe the transmission properties quantitatively, we define the following transmission coefficients

$$T \equiv \left|\frac{\alpha_{2,\text{out}}}{\alpha_{1,\text{in}}}\right|^2, \quad \tilde{T} \equiv \left|\frac{\tilde{\alpha}_{1,\text{out}}}{\tilde{\alpha}_{2,\text{in}}}\right|^2, \quad (9)$$

respectively, for the two cases with opposite transmission directions.

By making use of Eqs. (5) and (7), the transmission

coefficients are determined by

$$0 = 4U^2T^3s_{\text{in}}^2 - 8\Delta UT^2s_{\text{in}} + T(\kappa^2 + 4\Delta^2) - \lambda, \quad (10a)$$

$$0 = 4\tilde{U}^2\tilde{T}^3\tilde{s}_{\text{in}}^2 - 8\Delta\tilde{U}\tilde{T}^2\tilde{s}_{\text{in}} + \tilde{T}(\kappa^2 + 4\Delta^2) - \lambda \quad (10b)$$

with $s_{\text{in}} = |\alpha_{1,\text{in}}|^2$, $\tilde{s}_{\text{in}} = |\alpha_{2,\text{in}}|^2$, and $\lambda = 16J^2\kappa_{1,e}\kappa_{2,e}/(\kappa_2^2 + 4\Delta_2^2)$.

The optical nonreciprocity requires $T \neq \tilde{T}$ when the input fields have the same powers in the two cases, i.e. $p_{\text{in}} = \tilde{p}_{\text{in}}$ and $s_{\text{in}} = \tilde{s}_{\text{in}}$. Thus it is clear from Eqs. (10a) and (10b) that the necessary condition to observe the optical nonreciprocity is $U \neq \tilde{U}$, which can be explicitly written as

$$\kappa_{1,e}(\kappa_2^2 + 4\Delta_2^2) \neq 4\kappa_{2,e}J^2. \quad (11)$$

We would like to note that the similar condition of optical nonreciprocity has also been reported in Ref. [38] in a similar three-mode optomechanical system without the optical gain.

III. UNIDIRECTIONAL AMPLIFICATION

In this section we will study the transmission behavior in the three-mode optomechanical system under consideration. It is found that the optical signal field can be unidirectionally amplified with the additional optical gain. And the expressions of the optimal transmission coefficient and the isolation ratio are given analytically.

A. Stability condition

Since both the optical gain and the nonlinear interaction are introduced in our system, the first step is to ensure the stability of the system in steady state. By splitting each operator into its mean value and fluctuation: $a_j = \alpha_j + \delta a_j$, $q = \bar{q} + \delta q$, $p = \bar{p} + \delta p$, the linearized QLEs corresponding to Eqs. (2a)-(2d) can be written in a matrix form as

$$\dot{\mu} = -M\mu + \Gamma\mu_{\text{in}}, \quad (12)$$

where $\mu = (\delta a_1, \delta a_1^\dagger, \delta a_2, \delta a_2^\dagger, \delta p, \delta q)^T$, $\mu_{\text{in}} = (a_{1,\text{in}}^{(e)}, a_{1,\text{in}}^{(e)\dagger}, a_{1,\text{in}}^{(o)}, a_{1,\text{in}}^{(o)\dagger}, a_{2,\text{in}}^{(e)}, a_{2,\text{in}}^{(e)\dagger}, a_{2,\text{in}}^{(o)}, a_{2,\text{in}}^{(o)\dagger}, a_{1,\text{in}}^{(g)}, a_{1,\text{in}}^{(g)\dagger}, 0, \zeta)^T$, and the coefficient matrix

$$M = \begin{pmatrix} \frac{\kappa_{\text{eff}}}{2} + i(\Delta_1 + g\bar{q}) & 0 & iJ & 0 & ig\alpha_1 & 0 \\ 0 & \frac{\kappa_{\text{eff}}}{2} - i(\Delta_1 + g\bar{q}) & 0 & -iJ & -ig\alpha_1^* & 0 \\ iJ & 0 & \frac{\kappa_2}{2} + i\Delta_2 & 0 & 0 & 0 \\ 0 & -iJ & 0 & \frac{\kappa_2}{2} - i\Delta_2 & 0 & 0 \\ 0 & 0 & 0 & 0 & 0 & -\omega_m \\ g\alpha_1^* & g\alpha_1 & 0 & 0 & \omega_m & \gamma_m \end{pmatrix}, \quad (13)$$

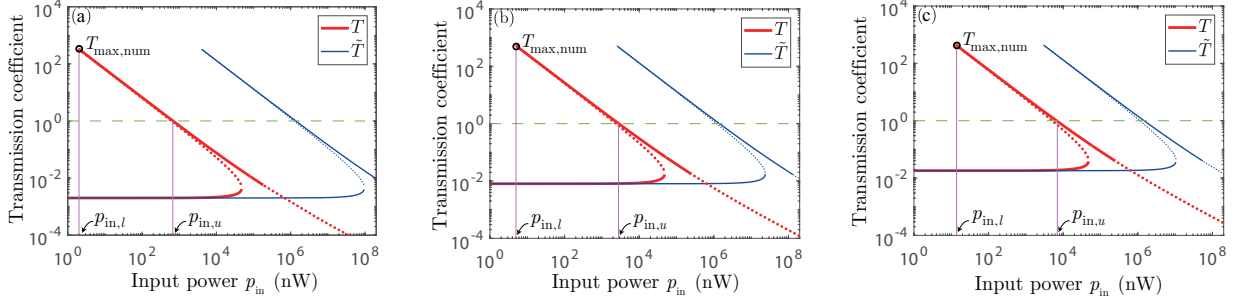


FIG. 2. (Color online) Transmission coefficients T (red) and \tilde{T} (blue) as a function of the input power p_{in} for (a) $J = 0.5J_0$, (b) $J = J_0$, and (c) $J = 1.5J_0$. $T_{\text{max,num}}$ (black circle) represents the maximum value of the transmission coefficient T obtained numerically. The solid (dotted) lines represent stable (unstable) values of T and \tilde{T} . The green dash line corresponding to $T = 1$ is the benchmark of amplification. The system shows clearly the working region of optical nonreciprocity is $p_{\text{in}} \in [p_{\text{in},l}, p_{\text{in},u}]$. Here the other parameters are chosen referring to the recent optomechanical experiment with whispering gallery [47]: $\kappa_1/2\pi = \kappa_2/2\pi = 100$ MHz, $\kappa_{\text{eff}}/2\pi = 200$ kHz, $\kappa_{1,e}/2\pi = \kappa_{2,e}/2\pi = 100$ MHz, $\omega_d/2\pi = 200$ THz, $\omega_m/2\pi = 200$ MHz, $\gamma_m/2\pi = 50$ kHz, $g/2\pi = 0.8$ kHz, $\Delta_1/2\pi = 50$ MHz, $\Delta_2/2\pi = 20$ MHz, and $J_0/2\pi = 2.41$ MHz.

$$\Gamma = \begin{pmatrix} \sqrt{\kappa_{1,e}} & 0 & \sqrt{\kappa_{1,o}} & 0 & 0 & 0 & 0 & 0 & \sqrt{\mathcal{G}} & 0 & 0 & 0 \\ 0 & \sqrt{\kappa_{1,e}} & 0 & \sqrt{\kappa_{1,o}} & 0 & 0 & 0 & 0 & 0 & \sqrt{\mathcal{G}} & 0 & 0 \\ 0 & 0 & 0 & 0 & \sqrt{\kappa_{2,e}} & 0 & \sqrt{\kappa_{2,o}} & 0 & 0 & 0 & 0 & 0 \\ 0 & 0 & 0 & 0 & 0 & \sqrt{\kappa_{2,e}} & 0 & \sqrt{\kappa_{2,o}} & 0 & 0 & 0 & 0 \\ 0 & 0 & 0 & 0 & 0 & 0 & 0 & 0 & 0 & 0 & 0 & 0 \\ 0 & 0 & 0 & 0 & 0 & 0 & 0 & 0 & 0 & 0 & 0 & \sqrt{2\gamma_m} \end{pmatrix}. \quad (14)$$

The stability condition can be derived by using the Routh-Hurwitz criterion [46], which requires all the real parts of eigenvalues of the matrix M to be positive. The explicit forms of such a criterion in the current model are cumbersome and not given here. However, in the following discussions all the stability conditions have been checked numerically.

B. Optical amplification induced by optical gain

For the nonreciprocal device based on the nonlinearity in the three-mode optomechanical system [38], the optical diode is achieved and the value of the maximum transmission coefficients is usually smaller than one. This subsection will show the optical unidirectional amplification assisted by the optical gain. That is, the transmission coefficient along one of the two directions is larger than one, and the one in the opposite direction is much smaller than one.

In Fig. 2, the transmission coefficients T and \tilde{T} are plotted as a function of the input power p_{in} . It is apparent that in Fig. 2 the optical unidirectional amplification appears in two regions where $T > 1 > \tilde{T}$ (i.e. $p_{\text{in}} \in [p_{\text{in},l}, p_{\text{in},u}]$) and $\tilde{T} > 1 > T$, respectively. However, the isolation ratio in the first region is better than that in the second region. Then in what follows, we just focus on the first region with $p_{\text{in}} \in [p_{\text{in},l}, p_{\text{in},u}]$, where we only

consider the upper branch of T .

As shown in Fig. 2(a), when the system works in the upper branch of T with $p_{\text{in}} \in [p_{\text{in},l}, p_{\text{in},u}]$, it has obvious optical nonreciprocity with the tremendous difference between the values of (upper-branch) T and \tilde{T} . Here, $p_{\text{in},l} = 2.03$ nW and $p_{\text{in},u} = 0.68$ μ W corresponding to $T = T_{\text{max,num}}$ and $T = 1$, respectively, are the lower and upper bounds of input field power.

To quantify optical nonreciprocity, the isolation ratio is introduced as E (dB) = $10 \times \log_{10}(T/\tilde{T})$. Accordingly, with $p_{\text{in}} \in [p_{\text{in},l}, p_{\text{in},u}]$ in Fig. 2(a), it is found numerically that $|E$ (dB)| $\in [26.99, 52.04]$. Moreover, in Fig. 2(a) the value of T is larger than 1 while that of \tilde{T} is much smaller than 1 in the working region. It clearly displays that the signal is amplified when the input field is injected from cavity 1. With the aid of the optical gain, Fig. 2(b) and Fig. 2(c) also show the similar unidirectional amplification as that in Fig. 2(a). Note that in Fig. 2, the parameters satisfy the nonreciprocity condition Eq. (11).

The effect of the external decay rate $\kappa_{1,e}$ on the transmission behavior is also investigated in Fig. 3. This figure shows that with the increase of $\kappa_{1,e}$, all the values of the transmission coefficients are collectively lifted upward. This means with the increase of the external decay in cavity 1, both the transmission coefficients in the two directions can be increased with the unidirectional amplification remained.

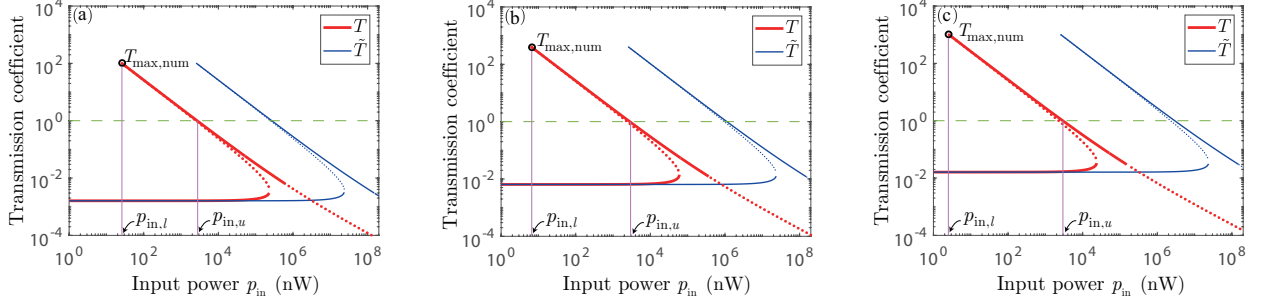


FIG. 3. (Color online) Transmission coefficients T (red) and \tilde{T} (blue) as a function of the input power p_{in} for (a) $\kappa_{1,e}/2\pi = 20$ MHz, (b) $\kappa_{1,e}/2\pi = 80$ MHz, and (c) $\kappa_{1,e}/2\pi = 200$ MHz. $T_{\text{max,num}}$ (the black circle) represents the maximum value of the transmission coefficient T obtained numerically. Here the other parameters are chosen referring to Ref. [47]: $\kappa_1/2\pi = 200$ MHz, $\kappa_2/2\pi = 100$ MHz, $\kappa_{\text{eff}}/2\pi = 200$ kHz, $\kappa_{2,e}/2\pi = 100$ MHz, $\omega_d/2\pi = 200$ THz, $\omega_m/2\pi = 200$ MHz, $\gamma_m/2\pi = 50$ kHz, $g/2\pi = 0.8$ kHz, $\Delta_1/2\pi = 50$ MHz, $J/2\pi = 2.19$ MHz, $\Delta_2/2\pi = 60$ MHz. Similar to Fig. 2, the solid (dotted) lines represent the stable (unstable) values for T and \tilde{T} , and the green dash line corresponding to $T = 1$ is the benchmark of amplification.

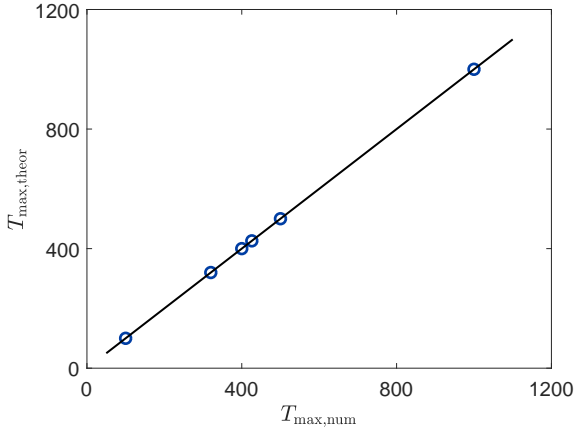


FIG. 4. (Color online) The black solid line represents the equation $T_{\text{max,num}} = T_{\text{max,theor}}$, and each blue circle denotes the point with the coordinates $(T_{\text{max,num}}, T_{\text{max,theor}})$ which are respectively obtained numerically and analytically for the same parameters. Actually these values of $T_{\text{max,num}}$ are taken from the data marked as black circles in Fig. 2 and Fig. 3, and that of $T_{\text{max,theor}}$ are calculated based on Eq. (17) with the corresponding parameters. One can find all the blue circles collapse into the line.

C. Optimal transmission coefficient and the corresponding isolation ratio

In Sec. III B, it is found that with $p_{\text{in}} \in [p_{\text{in},l}, p_{\text{in},u}]$, our optomechanical system displays the optical nonreciprocal transmission of unidirectional amplification. This inspires us to ask the following question: What are the optimal maximum transmission coefficient and the corresponding isolation ratio in our system? We will study such a question in details in this section.

Eq. (10a) is a cubic equation for the transmission coefficient T . However, the analytical solution of T has

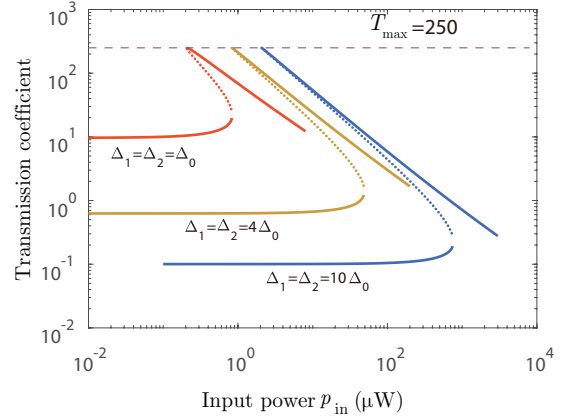


FIG. 5. (Color online) Transmission coefficients T as a function of the input power p_{in} for different values of the detuning. The dotted lines represent unstable values and solid lines represent stable values. The cavity coupling strength is kept to be the optimal one $J = J_{\text{opt}} \equiv \sqrt{\kappa_{\text{eff}}(\kappa_2^2 + \Delta_2^2)/(4\kappa_2)}$. Here the other parameters are chosen based on a recent optomechanical experiment with whispering gallery [47]: $\kappa_1/2\pi = 50$ MHz, $\kappa_2/2\pi = 100$ MHz, $\kappa_{\text{eff}}/2\pi = 200$ kHz, $\kappa_{1,e}/2\pi = 50$ MHz, $\kappa_{2,e}/2\pi = 100$ MHz, $\omega_d/2\pi = 200$ THz, $\omega_m/2\pi = 200$ MHz, $\gamma_m/2\pi = 50$ kHz, $g/2\pi = 0.8$ kHz, $\Delta_0/2\pi = 1$ MHz.

somewhat complex dependence on the system parameters and makes it less informative. This difficulty can be circumvented by solving s_{in} in Eq. (10a). The solution to s_{in} in Eq. (10a) is formally given as

$$s_{\text{in}} = \frac{2T\Delta \pm \sqrt{T\lambda - T^2\kappa^2}}{2T^2U}. \quad (15)$$

Because s_{in} must be positive, under the condition $\Delta > 0$, the valid region of T with $T\lambda - T^2\kappa^2 \geq 0$ should be

$$0 < T \leq T_{\text{max,theor}}, \quad (16)$$

where the possible maximum transmission coefficient

$$T_{\max, \text{theor}} = \frac{\lambda}{\kappa^2} = \frac{16J^2 \kappa_{1,e} \kappa_{2,e} (\kappa_2^2 + 4\Delta_2^2)}{[4J^2 \kappa_2 + \kappa_{\text{eff}} (\kappa_2^2 + 4\Delta_2^2)]^2}. \quad (17)$$

With the optical amplification requirement $T_{\max, \text{theor}} > 1$, the condition for κ_{eff} is determined as

$$0 < \kappa_{\text{eff}} < \sqrt{16J^2 \kappa_{1,e} \kappa_{2,e} (\kappa_2^2 + 4\Delta_2^2)} - \frac{4J^2 \kappa_2}{\kappa_2 + 4\Delta_2^2}. \quad (18)$$

The numerical counterpart $T_{\max, \text{num}}$ of the maximum transmission coefficient T_{\max} can be easily obtained by the numerical solutions to Eq. (10a), such as that in Fig. 2. For the parameters considered in Figs. 2-4, it is checked that the relation $T_{\max, \text{num}} = T_{\max, \text{theor}}$ is always valid in the working region. As an example, in Fig. 4 all the blue circles representing the point $(T_{\max, \text{num}}, T_{\max, \text{theor}})$ collapse into the line with equation $T_{\max, \text{num}} = T_{\max, \text{theor}}$. This suggests that the expression given in Eq. (17) is a good approximate result for T_{\max} for the parameters considered in Figs. 2-4. From now on, for simplicity we set $T_{\max} = T_{\max, \text{theor}}$.

Then, T_{\max} can be further optimized with respect to the coupling strength J between the two cavities. Solving $\partial T_{\max} / \partial J = 0$ under the condition $\kappa_{\text{eff}} > 0$, the optimal coupling strength is given as

$$J = J_{\text{opt}} := \sqrt{\frac{\kappa_{\text{eff}} (\kappa_2^2 + 4\Delta_2^2)}{4\kappa_2}}. \quad (19)$$

Substituting Eq. (19) into Eq. (17), the optimized value of T_{\max} is obtained as

$$T_{\max}^{\text{opt}} = \frac{\kappa_{1,e}}{\kappa_{\text{eff}}} \cdot \frac{\kappa_{2,e}}{\kappa_2}. \quad (20)$$

There are two terms in Eq. (20), in which the first (second) term represents the proportion of the external decay rate into the effective (total) decay of the cavity. This indicates that T_{\max}^{opt} is determined only by the intrinsic parameters of the system. As a result, T_{\max}^{opt} should remain as a constant, when the other parameters (e.g., the detunings) are changed. This invariance of T_{\max}^{opt} is displayed in Fig. 5: although the detuning Δ_1 and Δ_2 change, T_{\max}^{opt} is unaltered.

Finally, the isolation ratio E_0 corresponding to T_{\max}^{opt} is derived. According to Eqs. (10a, 10b, 19), the absolute value of isolation ratio is given as

$$|E_0| \simeq 10 \times \log_{10} \left(1 + \frac{(\kappa_2 \Delta_1 - \kappa_{\text{eff}} \Delta_2)^2}{\kappa_2^2 \kappa_{\text{eff}}^2} \right), \quad (21)$$

where we have used the fact that $T_{\max}^{\text{opt}} \gg 1$ and the corresponding value of \tilde{T} at $p_{\text{in}} = p_{\text{in}, l}$ is much less than 1. For the special case $\kappa_2 \gg \kappa_{\text{eff}}$ and $\Delta_1 \sim \Delta_2 \gg \kappa_{\text{eff}} > 0$, Eq. (21) is simplified as

$$|E_0| \simeq 10 \times \log_{10} \frac{\Delta_1^2}{\kappa_{\text{eff}}^2}. \quad (22)$$

That means one can obtain good isolation ratio by modifying the optical gain so that the effective decay rate κ_{eff} of cavity 1 is very small compared with κ_2 and $\Delta_{1,2}$.

IV. NOISE ANALYSIS

In this section, we will analyze the effect of the added noise in our proposal. For this, we resort to the linearized QLEs of operator fluctuations [i.e., Eq. (12)], which include the noise operators. In both cases that the input field is only injected into cavity 1 or cavity 2, Eq. (12) maintains the same expression except that the average values [e.g., α_1 , α_2 and \bar{q} in Eq. (13)] are different in different cases.

The solution to Eq. (12) in the frequency domain can be written as

$$\mu(\omega) = (M - i\omega I)^{-1} \Gamma \mu_{\text{in}}(\omega), \quad (23)$$

and the Fourier transform of any operator is introduced as

$$o(\omega) = \int_{-\infty}^{+\infty} o(t) e^{i\omega t} dt. \quad (24)$$

Then taking Eq. (23) into Eq. (4) in the Fourier domain, we obtain

$$\mu_{\text{out}}(\omega) = \mathcal{T}(\omega) \mu_{\text{in}}(\omega), \quad (25)$$

where $\mu_{\text{out}} = (a_{1,\text{out}}^{(e)}, a_{1,\text{out}}^{(e)\dagger}, a_{1,\text{out}}^{(o)}, a_{1,\text{out}}^{(o)\dagger}, a_{2,\text{out}}^{(e)}, a_{2,\text{out}}^{(e)\dagger}, a_{2,\text{out}}^{(o)}, a_{2,\text{out}}^{(o)\dagger}, a_{1,\text{out}}^{(\mathcal{G})}, a_{1,\text{out}}^{(\mathcal{G})\dagger}, 0, \zeta)^T$, and the scattering matrix is

$$\mathcal{T}(\omega) = \Gamma^T (M - i\omega I)^{-1} \Gamma - I. \quad (26)$$

The element of the scattering matrix \mathcal{T}_{ij} ($i, j = 1, 2, \dots, 7$) represents the transmission amplitude of the j th element in $\mu_{\text{in}}(\omega)$ to the i th element in $\mu_{\text{out}}(\omega)$.

To calculate the output spectra, we use the non-zero correlation functions of the input noise operators in Eq. (23) as the followings

$$\langle a_{j,\text{in}}^{(e)}(\omega) a_{j,\text{in}}^{(e)\dagger}(\omega') \rangle = 2\pi \delta(\omega + \omega'), \quad (27a)$$

$$\langle a_{j,\text{in}}^{(o)}(\omega) a_{j,\text{in}}^{(o)\dagger}(\omega') \rangle = 2\pi \delta(\omega + \omega'), \quad (27b)$$

$$\langle a_{1,\text{in}}^{(\mathcal{G})\dagger}(\omega) a_{1,\text{in}}^{(\mathcal{G})}(\omega') \rangle = 2\pi \delta(\omega + \omega'), \quad (27c)$$

$$\langle \zeta(\omega) \zeta(\omega') \rangle = 2\pi (n_m + \frac{1}{2}) \delta(\omega + \omega'). \quad (27d)$$

Here, the thermal photon numbers have been taken to be zero as the frequencies of the cavities are very high (e.g., of the order of 10^{14} Hz), however the thermal phonon number is given as $n_m = 1/[\exp(\hbar\omega_m/k_B T) - 1]$, where k_B is the Boltzmann constant and T is the effective temperature of the reservoir.

Then the output spectra of cavity 2 in the first case, where the input field is only injected into cavity 1, can be obtained as [29]

$$S_{2,\text{out}}(\omega) = \frac{1}{2} \int \frac{d\omega'}{2\pi} \left\langle a_{2,\text{out}}(\omega) a_{2,\text{out}}^\dagger(\omega') + a_{2,\text{out}}^\dagger(\omega') a_{2,\text{out}}(\omega) \right\rangle$$

$$= S_{1,e} + S_{1,o} + S_{2,e} + S_{2,o} + S_G + S_m \quad (28)$$

with

$$S_{1,e} = \frac{1}{2} [\mathcal{T}_{5,1}(\omega) \mathcal{T}_{6,2}(-\omega) + \mathcal{T}_{6,1}(\omega) \mathcal{T}_{5,2}(-\omega)], \quad S_{1,o} = \frac{1}{2} [\mathcal{T}_{5,3}(\omega) \mathcal{T}_{6,4}(-\omega) + \mathcal{T}_{6,3}(\omega) \mathcal{T}_{5,4}(-\omega)], \quad (29a)$$

$$S_{2,e} = \frac{1}{2} [\mathcal{T}_{5,5}(\omega) \mathcal{T}_{6,6}(-\omega) + \mathcal{T}_{6,5}(\omega) \mathcal{T}_{5,6}(-\omega)], \quad S_{2,o} = \frac{1}{2} [\mathcal{T}_{5,7}(\omega) \mathcal{T}_{6,8}(-\omega) + \mathcal{T}_{6,7}(\omega) \mathcal{T}_{5,8}(-\omega)], \quad (29b)$$

$$S_G = \frac{1}{2} [\mathcal{T}_{5,10}(\omega) \mathcal{T}_{6,9}(-\omega) + \mathcal{T}_{6,10}(\omega) \mathcal{T}_{5,9}(-\omega)], \quad S_m = \mathcal{T}_{5,12}(\omega) \mathcal{T}_{6,12}(-\omega) \left(n_m + \frac{1}{2} \right), \quad (29c)$$

where $S_{j,e}$ and $S_{j,o}$ ($j = 1, 2$) represent the effects of the external and internal noises to cavity j rising from the optical vacuum fluctuations, respectively; S_G stands for the effect of the noise originating from the optical gain; S_m represents the effect of the thermal noise to the mechanical modes.

Now we define noise-to-signal ratio (NSR) in the first case as the ratio of the integral of the output spectra $S_{2,\text{out}}(\omega)$ and the output signal amplitude $|\alpha_{2,\text{out}}|^2$ to describe the quantity of the added noise in the output port [41]. Experimentally, the noise under consideration will be detected by a measurement device with a small bandwidth $2\Delta\omega$ around $\omega = 0$, in this case NSR can be

defined by [30, 41]

$$\text{NSR} := \frac{1}{|\alpha_{2,\text{out}}|^2} \int_{-\Delta\omega}^{\Delta\omega} d\omega S_{2,\text{out}}(\omega). \quad (30)$$

Similarly, in the second case that the input filed is only injected into cavity 2, we can accordingly define $\widetilde{\text{NSR}}$ to describe the quantity of the added output noise as

$$\widetilde{\text{NSR}} := \frac{1}{|\tilde{\alpha}_{1,\text{out}}|^2} \int_{-\Delta\omega}^{\Delta\omega} d\omega \tilde{S}_{1,\text{out}}(\omega), \quad (31)$$

where

$$\tilde{S}_{1,\text{out}}(\omega) = \frac{1}{2} \int \frac{d\omega'}{2\pi} \left\langle \tilde{a}_{1,\text{out}}(\omega) \tilde{a}_{1,\text{out}}^\dagger(\omega') + \tilde{a}_{2,\text{out}}^\dagger(\omega') \tilde{a}_{2,\text{out}}(\omega) \right\rangle$$

$$= \tilde{S}_{1,e} + \tilde{S}_{1,o} + \tilde{S}_{2,e} + \tilde{S}_{2,o} + \tilde{S}_G + \tilde{S}_m \quad (32)$$

with

$$\tilde{S}_{1,e} = \frac{1}{2} \left(\tilde{\mathcal{T}}_{1,1}(\omega) \tilde{\mathcal{T}}_{2,2}(-\omega) + \tilde{\mathcal{T}}_{2,1}(\omega) \tilde{\mathcal{T}}_{1,2}(-\omega) \right), \quad \tilde{S}_{1,o} = \frac{1}{2} \left(\tilde{\mathcal{T}}_{1,3}(\omega) \tilde{\mathcal{T}}_{2,4}(-\omega) + \tilde{\mathcal{T}}_{2,3}(\omega) \tilde{\mathcal{T}}_{1,4}(-\omega) \right) \quad (33a)$$

$$\tilde{S}_{2,e} = \frac{1}{2} \left(\tilde{\mathcal{T}}_{1,5}(\omega) \tilde{\mathcal{T}}_{2,6}(-\omega) + \tilde{\mathcal{T}}_{2,5}(\omega) \tilde{\mathcal{T}}_{1,6}(-\omega) \right), \quad \tilde{S}_{2,o} = \frac{1}{2} \left(\tilde{\mathcal{T}}_{1,7}(\omega) \tilde{\mathcal{T}}_{2,8}(-\omega) + \tilde{\mathcal{T}}_{2,7}(\omega) \tilde{\mathcal{T}}_{1,8}(-\omega) \right) \quad (33b)$$

$$\tilde{S}_G = \frac{1}{2} \left(\tilde{\mathcal{T}}_{1,10}(\omega) \tilde{\mathcal{T}}_{2,9}(-\omega) + \tilde{\mathcal{T}}_{2,10}(\omega) \tilde{\mathcal{T}}_{1,9}(-\omega) \right), \quad \tilde{S}_m = \tilde{\mathcal{T}}_{1,12}(\omega) \tilde{\mathcal{T}}_{2,12}(-\omega) \left(n_m + \frac{1}{2} \right). \quad (33c)$$

For the reason that the analytical expressions of Eq. (30) and Eq. (31) are so complex, we numerically display NSR ($\widetilde{\text{NSR}}$) as a function of the input power p_{in} in Fig. 6. In the following simulations, we take the typical bandwidth $\Delta\omega/2\pi = 30$ Hz as in the current experimental condition [30]. Moreover, in order to clearly display the impact of the added noise on optical directional amplification, we only focus on the added noise of the system working on the upper branch of T and the lower branch of \tilde{T} with $p_{\text{in}} \in [p_{\text{in},l}, p_{\text{in},u}]$ in Fig. 2(b).

As shown in Fig. 6, the maximum value of either NSR or $\widetilde{\text{NSR}}$ is smaller than 10^{-6} in the working region in

Fig. 2(b). This means that the effects of the added noise in our proposal of optical nonreciprocal transmission with unidirectional amplification can be ignored.

V. CONCLUSIONS

In summary, it is found that assisted by the optical gain, the nonreciprocal transmission with unidirectional amplification can be realized for a strong optical input signal in our three-mode optomechanical system. The origin of the optical amplification comes from the optical

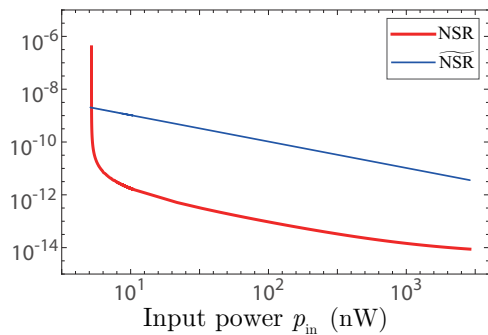


FIG. 6. (Color online) NSR (red line) and $\widetilde{\text{NSR}}$ (blue line) as a function of the input power p_{in} . We only plot NSR on the situation that the system works on the upper branch of T and the lower branch of $\widetilde{\text{NSR}}$. The region of the input power p_{in} is the working region in Fig. 2(b), where $p_{\text{in}} \in [5.2 \text{ nW}, 2.83 \mu\text{W}]$. Here $n_m = 100$, $\Delta\omega/2\pi = 30 \text{ Hz}$, and the other parameters are the same as that in Fig. 2(b).

gain. An interesting property of our system is that it si-

multaneously has high isolation ratio and high transmission coefficient in a particular direction. Furthermore, the expressions for the optimal transmission coefficient in the amplified direction and the corresponding isolation ratio are analytically obtained. However, there is a fact that should be stressed: the unidirectional amplification in our system is sensitive to the power of input signal field, and overcoming this issue is a new question and needs a future study.

VI. ACKNOWLEDGMENTS

This work was supported by the Science Challenge Project (under Grant No. TZ2018003), the National Key R&D Program of China under Grant No. 2016YFA0301200, the National Natural Science Foundation of China (under Grants No. 11774024, No. 11534002, No. 11874170, No. 11604096, No. U1930402, and No. U1730449), and the Postdoctoral Science Foundation of China (under Grant No. 2017M620593).

-
- [1] M. Aspelmeyer, T. J. Kippenberg, and F. Marquardt, Cavity optomechanics, *Rev. Mod. Phys.* **86**, 1391 (2014).
 - [2] G. S. Agarwal and S. Huang, Electromagnetically induced transparency in mechanical effects of light, *Phys. Rev. A* **81**, 041803 (2010).
 - [3] S. Weis, R. Rivière, S. Deléglise, E. Gavartin, O. Arcizet, A. Schliesser, and T. J. Kippenberg, Optomechanically induced transparency, *Science* **330**, 1520 (2010).
 - [4] A. H. Safavi-Naeini, T. P. Mayer Alegre, J. Chan, M. Eichenfield, M. Winger, Q. Lin, J. T. Hill, D. E. Chang, and O. Painter, Electromagnetically induced transparency and slow light with optomechanics, *Nature (London)* **472**, 69 (2011).
 - [5] L. Tian, Robust photon entanglement via quantum interference in optomechanical interfaces, *Phys. Rev. Lett.* **110**, 233602 (2013).
 - [6] Y. D. Wang and A. A. Clerk, Reservoir-engineered entanglement in optomechanical systems, *Phys. Rev. Lett.* **110**, 253601 (2013).
 - [7] I. Marinković, A. Wallucks, R. Riedinger, S. Hong, M. Aspelmeyer, and S. Gröblacher, Optomechanical Bell test, *Phys. Rev. Lett.* **121**, 220404 (2018).
 - [8] J. Margueritat, A. V. Carlotta, S. Monnier, H. D. Ayari, H. C. Mertani, A. Berthelot, Q. Martinet, X. Dagany, C. Rivière, J. P. Rieu, and T. Dehoux, High-frequency mechanical properties of tumors measured by Brillouin light scattering, *Phys. Rev. Lett.* **122**, 018101 (2019).
 - [9] L. J. Aplet and J. W. Carson, A Faraday effect optical isolator, *Appl. Opt.* **3**, 544 (1964).
 - [10] C. W. Peterson, W. A. Benalcazar, M. Lin, T. L. Hughes, and G. Bahl, Strong nonreciprocity in modulated resonator chains through synthetic electric and magnetic fields, *arXiv: 1903.07408*.
 - [11] H. Lira, Z. Yu, S. Fan, and M. Lipson, Electrically driven nonreciprocity induced by interband photonic transition on a silicon chip, *Phys. Rev. Lett.* **109**, 033901 (2012).
 - [12] K. Fang, Z. Yu, and S. Fan, Photonic Aharonov-Bohm effect based on dynamic modulation, *Phys. Rev. Lett.* **108**, 153901 (2012).
 - [13] R. Fleury, D. L. Sounas, C. F. Sieck, M. R. Haberman, and A. Alù, Sound isolation and giant linear nonreciprocity in a compact acoustic circulator, *Science* **343**, 516 (2014).
 - [14] D. L. Sounas, C. Caloz, and A. Alù, Giant nonreciprocity at the subwavelength scale using angular momentum-biased metamaterials, *Nat. Commun.* **4**, 2407 (2013).
 - [15] N. A. Estep, D. L. Sounas, J. Soric, and A. Alù, Magnetic-free non-reciprocity and isolation based on parametrically modulated coupled-resonator loops, *Nat. Phys.* **10**, 923 (2014).
 - [16] D. W. Wang, H. T. Zhou, M. J. Guo, J. X. Zhang, J. Evers, and S. Y. Zhu, Optical diode made from a moving photonic crystal, *Phys. Rev. Lett.* **110**, 093901 (2013); S. A. R. Horsley, J. H. Wu, M. Artoni, and G. C. La Rocca, Optical nonreciprocity of cold atom Bragg mirrors in motion, *Phys. Rev. Lett.* **110**, 223602 (2013).
 - [17] M. Hafezi and P. Rabl, Optomechanically induced nonreciprocity in microring resonators, *Opt. Express* **20**, 7672 (2012).
 - [18] Z. Shen, Y. L. Zhang, Y. Chen, C. L. Zou, Y. F. Xiao, X. B. Zou, F. W. Sun, G. C. Guo, and C. H. Dong, Experimental realization of optomechanically induced nonreciprocity, *Nat. Photon.* **10**, 657 (2016).
 - [19] H. Jing, S. K. Özdemir, Z. Geng, J. Zhang, X. Y. Lü, B. Peng, L. Yang, and F. Nori, Optomechanically-induced transparency in parity-time-symmetric microresonators, *Sci. Rep.* **5**, 9663 (2015).
 - [20] L. Tian and Z. Li, Nonreciprocal quantum-state conversion between microwave and optical photons, *Phys. Rev.*

- A **96**, 013808 (2017).
- [21] C. F. Ockeloen-Korppi, E. Damskäg, J. M. Pirkkalainen, T. T. Heikkilä, F. Massel, and M. A. Sillanpää, Low-noise amplification and frequency conversion with a multiport microwave optomechanical device, *Phys. Rev. X* **6**, 041024 (2016).
 - [22] D. Malz, L. D. Tóth, N. R. Bernier, A. K. Feofanov, T. J. Kippenberg, and A. Nunnenkamp, Quantum-limited directional amplifiers with optomechanics, *Phys. Rev. Lett.* **120**, 023601 (2018).
 - [23] K. Fang, J. Luo, A. Metelmann, M. H. Matheny, F. Marquardt, A. A. Clerk, and O. Painter, Generalized non-reciprocity in an optomechanical circuit via synthetic magnetism and reservoir engineering, *Nat. Phys.* **13**, 465 (2017).
 - [24] X. Z. Zhang, L. Tian, and Y. Li, Optomechanical transistor with mechanical gain, *Phys. Rev. A* **97**, 043818 (2018) (2018).
 - [25] C. Jiang, L. N. Song, and Y. Li, Directional amplifier in an optomechanical system with optical gain, *Phys. Rev. A* **97**, 053812 (2018).
 - [26] C. F. Ockeloen-Korppi, T. T. Heikkilä, M. A. Sillanpää, and F. Massel, Theory of phase-mixing amplification in an optomechanical system, *Quantum Sci. Technol.* **2**, 035002 (2017).
 - [27] Z. Shen, Y. L. Zhang, Y. Chen, F. W. Sun, X. B. Zou, G. C. Guo, C. L. Zou, and C. H. Dong, Reconfigurable optomechanical circulator and directional amplifier, *Nat. Commun.* **9**, 1797 (2018).
 - [28] Y. Li, Y. Y. Huang, X. Z. Zhang, and L. Tian, Optical directional amplification in a three-mode optomechanical system, *Opt. Express* **25**, 18907 (2017).
 - [29] A. Metelmann and A. A. Clerk, Nonreciprocal photon transmission and amplification via reservoir engineering, *Phys. Rev. X* **5**, 021025 (2015); A. Metelmann and A. A. Clerk, Quantum-limited amplification via reservoir engineering, *Phys. Rev. Lett.* **112**, 133904 (2014).
 - [30] L. M. de Lépinay, E. Damskäg, C. F. Ockeloen-Korppi, and M. A. Sillanpää, Realization of directional amplification in a microwave optomechanical device, *Phys. Rev. Appl.* **11**, 034027 (2019).
 - [31] A. Nunnenkamp, V. Sudhir, A. K. Feofanov, A. Roulet, and T. J. Kippenberg, Quantum-limited amplification and parametric instability in the reversed dissipation regime of cavity optomechanics, *Phys. Rev. Lett.* **113**, 023604 (2014).
 - [32] S. Manipatruni, J. T. Robinson, and M. Lipson, Optical nonreciprocity in optomechanical structures, *Phys. Rev. Lett.* **102**, 213903 (2009).
 - [33] A. S. Zheng, G. Y. Zhang, H. Y. Chen, T. T. Mei and J. B. Liu, Nonreciprocal light propagation in coupled microcavities system beyond weak-excitation approximation, *Sci. Rep.* **7**, 14001 (2017).
 - [34] L. N. Song, Z. H. Wang, and Y. Li, Enhancing optical nonreciprocity by an atomic ensemble in two coupled cavities, *Opt. Commun.* **415**, 39-42 (2018).
 - [35] S. C. Zhang, Y. Q. Hu, G. W. Lin, Y. P. Niu, K. Y. Xia, J. B. Gong and S. Q. Gong, Thermal-motion-induced non-reciprocal quantum optical system, *Nat. Photon.* **12**, 744 (2018).
 - [36] F. Ruesink, M.-A. Miri, A. Alù, and E. Verhagen, Non-reciprocity and magnetic-free isolation based on optomechanical interactions, *Nat. Commun.* **7**, 13662 (2016).
 - [37] S. R. K. Rodriguez, V. Goblots, N. Carlon Zambon, A. Amo, and J. Bloch, Nonreciprocity and zero reflection in nonlinear cavities with tailored loss, *Phys. Rev. A* **99**, 013850 (2019).
 - [38] X. W. Xu, L. N. Song, Q. Zheng, Z. H. Wang, and Y. Li, Optomechanically induced nonreciprocity in a three-mode optomechanical system, *Phys. Rev. A* **98**, 063845 (2018).
 - [39] X. Huang and S. Fan, Complete all-optical silica fiber isolator via Stimulated Brillouin Scattering, *J. Lightwave Technol.* **29**, 2267-2275 (2011).
 - [40] C. G. Poulton, R. Pant, A. Byrnes, S. Fan, M. J. Steel, and B. J. Eggleton, Design for broadband on-chip isolator using stimulated Brillouin scattering in dispersion-engineered chalcogenide waveguides, *Opt. Express* **20**, 21235-21246 (2012).
 - [41] N. T. Otterstrom, E. A. Kittlaus, S. Gertler, R. O. Behunin, A. L. Lentine, and P. T. Rakich, Resonantly enhanced nonreciprocal silicon Brillouin amplifier, *arXiv*: 1903.03907.
 - [42] L. Chang, X. Jiang, S. Hua, C. Yang, J. Wen, L. Jiang, G. Li, G. Wang, and M. Xiao, Parity-time symmetry and variable optical isolation in active-passive-coupled microresonators, *Nat. Photon.* **8**, 524 (2014).
 - [43] T. J. Kippenberg and K.J. Vahala, Cavity optomechanics, *Opt. Express* **15**, 17172 (2007).
 - [44] B. Peng, Ş. K. Özdemir, F. Lei, F. Monifi, M. Gianfreda, G. L. Long, S. Fan, F. Nori, C. M. Bender, and L. Yang, Parity-time-symmetric whispering-gallery microcavities, *Nat. Phys.* **10**, 394 (2014).
 - [45] C. W. Gardiner and M. J. Collett, Input and output in damped quantum systems: Quantum stochastic differential equations and the master equation, *Phys. Rev. A* **31**, 3761 (1985).
 - [46] E. X. DeJesus and C. Kaufman, Routh-Hurwitz criterion in the examination of eigenvalues of a system of nonlinear ordinary differential equations, *Phys. Rev. A* **35**, 5288 (1987).
 - [47] Y. Liu, M. Davanço, V. Aksyuk, and K. Srinivasan, Electromagnetically induced transparency and wideband wavelength conversion in silicon nitride microdisk optomechanical resonators, *Phys. Rev. Lett.* **110**, 223603 (2013).